The Influence of Electromagnetic Vibration on the Microstructure and Corrosion Behavior of Incoloy 825 Superalloy Weld Metal

A. Pourjafar[1], R. Dehmolaei[1,*]

[1]Department of Materials Science and Engineering, Faculty of Engineering, Shahid Chamran University of Ahvaz, Ahvaz, Iran.

Received: 28 May 2017 - Accepted: 6 August 2017

Abstract

In this study, the microstructure and corrosion behavior of Incoloy 825 superalloy weld joints were investigated. All the weld joints were produced by GTAW process with simultaneous applying of electromagnetic vibration under the voltages 0-30 Volts the microstructure of the base and weld metals in different welding conditions using optical and scanning electron microscopy was investigated. The corrosion behavior of weld metal using the cyclic polarization test was evaluated. Microscopic images were shown that the weld metals having a fully austenitic matrix contain fine precipitations on the grain boundaries and inside the grains. Increasing the applied vibration intensity causes decreased the distance between dendrites arms and augmentation of fine equiaxed dendrites and the refined grains in the weld metal. Furthermore, it was found that the vibration led to better distribution and refining precipitations in weld metal. The corrosion test results showed that employing electromagnetic vibration improves resistance to corrosion. The least resistance to corrosion (E_{pit}-E_{cor}) was 555.04 mV, which was related to the No-vibration welded joints, and the most resistance to corrosion was 1025.91 mV that was related to vibrated weld metal with 30 V.

Keywords: Incoloy 825, Microstructure, Electromagnetic Vibration, Cyclic Polarization, Corrosion.

1. Introduction

Superalloys are widely used in high temperature environments, such as steam generators, reformer, and pyrolysis tubes in oil refineries, petrochemical factories, and nuclear power plants, where a combination of strength and resistance to corrosion is required [1-7]. Incoloy 825 is one of Iron-nickel base superalloys which preserves good mechanical properties and resistance to corrosion in high temperature. Therefore, this alloy is used in highly corrosive environments such as oil and gas wells, nuclear industry, constructing pipes for environments containing sulfuric acid and phosphoric acid [3, 4], sea water, and reducer solutions [8, 9]. The weldability of this alloy due to the existence of austenite phase and high amount of Nickel and Chromium in its composition is good [7, 10-11].

Sindo Kou [12] showed that the solidification microstructure of weld metal and grain size has a drastic effect on the mechanical properties and sensitivity to hot cracking. He showed that vibration and stirring of weld molten pool are strongly effective on the solidification microstructure and mode of weld metal implementing an optimized vibration can play a key role in the modifying solidification structure, improvement of mechanical properties, and decreasing of sensitivity to hot solidification cracking of weld metal.

Bellezze et al. [13] for Incoloy 825 alloy showed that vibration caused the finer grains and uniform distribution of alloy elements in the structure. Therefore, it provides a more appropriate condition for forming of passive layer oxides. By increasing the velocity of oxide formation metal to obtain the passive condition again and it prevents growing of the created pit. In addition, decreasing in grain size and eliminating of inclusions and pits, due to vibration, causes a decrease in corrosion current [13]. Manning et al. [14], Cardareli et al. [15] by comparing the resistance to corrosion of Nickel base alloys and stainless steels illustrated that the sensitivity of these alloys was due to the producing of $M_{23}C_6$ carbides and depletion of grain boundaries from Chromium, produced from $M_{23}C_6$ depositions. They showed that for stabilizing this alloy, the prevention of this phenomenon is helpful.

Aytekin et al. [9] by studying the effect of coating on Incoloy 825 alloy showed that uniform corrosion, pitting, sensitivity and intergranular corrosion are some dangers which may exist in environments containing Chloride and Fluoride ions. Mesmari et al. [16] also showed that Nickel alloys, due to passive film formation, have great resistance to corrosion in corrosive environments.

Balasubramanian et al. [17], Kou [12] investigated the effect of vibration on the solidification mode of austenite stainless steel weld metal. It was found that vibration by Alternating Current (AC) resulted in applying Lorentz force to weld pool and vibrates

*Corresponding author
Email address: dehmolaei@scu.ac.ir

melt with the same frequency. Moreover, turbulence and stirring of weld pool causes increasing dendrite tips fragmentation, detaching partial melting grains, and decreasing the temperature causes more and better stability of fragmented dendrite tips and detached grains and heterogeneous nucleation place in the weld pool.

In this paper, Incoloy 825 superalloy was welded using the GTAW process and Inconel 82 as the filler metal. Electromagnetic vibration with various intensity is implemented during welding. The effects of electromagnetic vibration on microstructure and corrosion behavior of weld metal were investigated.

2. Materials and Methods

In this study, Incoloy 825 superalloy with 8mm thickness as the base metal and Inconel 82 (ER Ni-Cr-3) with 2.4mm diameter as the filler metal were used. The chemical composition of base and filler metals are shown in Table 1.

Some specimens with 50×100 mm dimensions of base metal were prepared. All Butt joints were provided in 35º V-groves and root distance and height equal to 2mm and 1mm, respectively. The specimens were welded using Tungsten arc method with Argon shielding gas, straight polarity (GTAW-DCEN), and without preheating. One of the specimens was welded without electromagnetic vibration and the others were welded under concurrent applying electromagnetic vibration in Voltages 12, 20, and 30 Volts. A schematic view of the electromagnetic vibration apparatus was shown in Fig. 1.

To investigate the microstructure of base and weld metals, the specimens of 10×20 mm were cut from welded samples so that weld bead was in the middle of them. The microstructure of weld metal using the optical microscope and scanning electron microscope (SEM-MIRA3TESCAN-XMU) equipped with EDS point analysis, was investigated. The cut specimen's surfaces were ground on silicon carbide paper of 60 to 3000 grits and finally, they were polished with a nylon cloth with 0.25 µm diamond paste. The specimens were electro-etched using Oxalic acid solution with 20 V for 15 S .The precipitates studies of unetched specimens were carried out at 1000× magnification using optical microscope.

To evaluate the corrosion behavior of weld metals, the cyclic potentiodynamic test for all of produced joints was carried out. After degreasing, a groove at the end of samples was created and a single-strand copper wire was placed in the groove by impact and then the samples were mounted using epoxy. In the cyclic potentiodynamic test, Saturated Calomel Electrode (SCE) as reference electrode and Platinum Electrode were used as counter electrodes. To reach the open Circuit Potential (OCP) steady state, the samples were kept in electrolyte for one hour, while the scanning rate was1 mV/s. Moreover, NaCl solution with 3.5% concentration was used as corrosive solution. The potential range for all samples from -500 to +1000 mV respect to OCP was considered. In all tests, E_{pit}-E_{corr} as a criterion for evaluating the resistance to pitting corrosion was used.

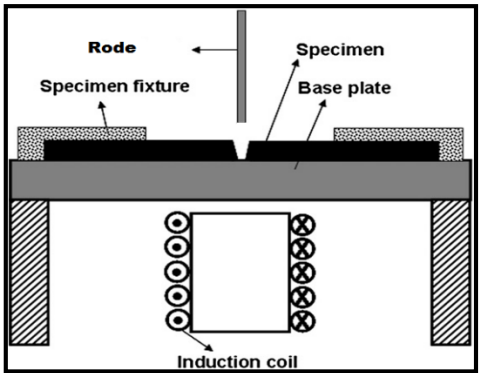

Fig. 1. A schematic view of electromagnetic vibration machine.

3. Results and Discussion

3.1. Microstructure

Fig. 2. shows the microstructure of Incoloy 825 base metal. The optical image (Fig. 2a) shows the fully austenitic equiaxed matrix containing two types of precipitates. These precipitates are found in the austenitic matrix and along the grain boundaries [18, 19]. Incoloy 825 contains 0.75% Titanium and 0.03% Carbon and hence tends to form Titanium Carbide and Titanium Nitride or Carbonitride during elevated temperature exposure [10, 11]. The SEM image (Fig. 2b) shows two different precipitates; First is the large precipitate with cubical morphology in the austenitic matrix and along the grain boundaries that might be Titanium Carbide formed during the solidification process; second is the fine precipitate with nearly spherical morphology and white color, probably Titanium Carbides [10, 11].These results confirmed by EDS analysis (Fig. 2c and d). Similar results have been also reported by others [20, 21].

Table 1. Chemical composition of filler and base metal (wt. %)[4].

Chemical analysis	C	Fe	Ni	Cr	Cu	Co	Mo	P	Nb	Ti	Si	S	Mn
Incoloy825	0.03	31.45	43.37	19.65	1.51	0.74	2.13	0	0.06	0.75	0.13	0	0.21
Inconel82	0.10	3.00	67.00	18.00 – 22.00	0.50	0	0	0.30	2.00 – 3.00	0.75	0.50	0.15	2.50 -3.50

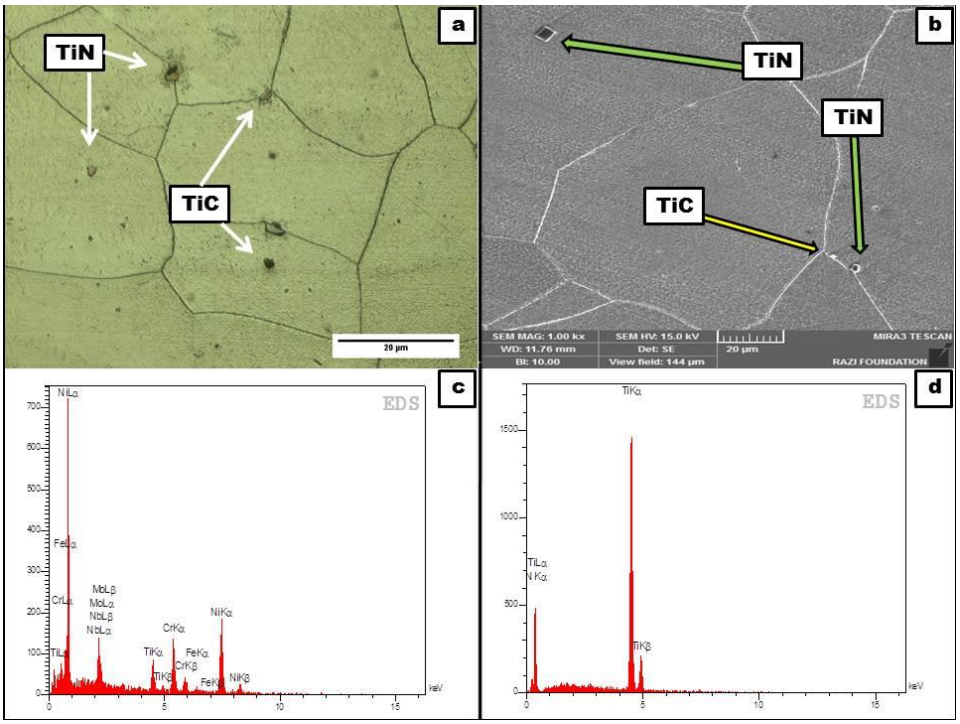

Fig. 2. a) Image of optical microscope of Incoloy 825, b) The SEM image of Incoloy 825, c) Chemical analysis of sinter TiN, d) Chemical analysis of sinter TiC.

The microstructure of the weld metal in vibrating voltages 0-30 Volts are shown in Fig. 3. It was observed the weld metal microstructure is completely austenitic with dendritic morphology. The grain growth orientation in grain boundaries is diverse and the competitive growth between different grains was occurred. It is shown in Fig. 3a that the structure of grains of weld metal before vibration is coarse columnar and equiaxed dendrites. Fig. 3 (b-d) reveals that electromagnetic vibration leads to fine grains and the tendency of the structure towards fine equiaxed dendrites. Furthermore, it was found that the finest structure relates to the weld joint which electromagnetic vibration with 30 V applied (Fig. 3d).

The microscopic images of the base and weld metals in the different welding conditions for unetched conditions are shown in Fig. 4 (a-d). The volume fraction and precipitates size were analyzed using image pro-plus software and the results are summarized in Table 2. The area fraction of precipitates considered over 10 mm^2 of the weld metal area.

The results of image analysis from dendrite length and the distance between dendrite arms in different specimens are shown in Table 2. As seen in Table 2. , it is deduced that applying electromagnetic vibration, the average length and width of the finest dendrite and the average of dendrites arm space from 38.86 µm,8.94µm and 12.32µm in welded specimens without vibration are declined to 6.05 µm, 2.09 µm and 3.01 µm in the specimens by applying vibration under 30 V, respectively. This topic indicates the tendency of the structure to be finer and transferring to fine equiaxed structure, particularly in the weld metal center by the increasing of electromagnetic vibration.

On the other hand, Table 2. shows that the smallest size (0.17 µm)and volume fraction (about 3.06%) of precipitates is in the produced weld metal by high vibration (30V), and the highest size (0.79) and volume fraction (about 26.02%) of precipitates is in the produced weld metal without vibration (0V).

Fig.4. shows the size and distribution of precipitates in different weld joints. From fig .4a observes more number and volume fraction of precipitates and agglomeration behavior. These images (b, c and d) exhibit that the increasing of electromagnetic vibration causes decreased the size and more uniform distribution of precipitates. The turbulence and weld pool stirring due to the vibration cause more uniform distribution of precipitates. Vibration causes the decreasing of weld pool temperature and increasing the thermal gradient. Therefore, time of precipitates growth decreases, as a result precipitates will be finer.

The vibration due to influence on the two main factors, including constitutional super cooling and increase in heterogeneous nucleation places, plays an important role in forming microstructures. The vibration causes, the molten easily moved in the weld pool and penetrates between dendrites. The molten pool movement causes increasing dendrite tips fragmentation in mushy zone and detaching

partial melted grains near the fusion liner and their migration to the weld pool. Dendrite tips and arms, due to conflict with adjacent arms and melts flow, are fragmented and cause the formation of preferential heterogeneous nucleation sites. Furthermore, the turbulence and weld pool stirring cause decreasing the temperature of weld pool and increasing the thermal gradient; the lowering temperature of weld pool causes the increasing of constitutional undercooling and decreasing the superheat and consequently it leads to stabilizing new nucleus and more heterogeneous nucleation as well as distance reduction between dendritic arms (Fig. 3d) [22-23]. In this case, the dominant mechanism of the grains refining is dendrites tips fragmentation. [12, 24-26].In the high vibration, due to highly turbulence in molten, the fluid flow and convection increase and facilitating the detachment of partial molted grains from base metal, and so causes cooling rate and lowering the molten temperature therefore, increasing the cooling rate causes decreasing the distance between dendrite arms from fusion line towards weld metal center line and consequently, results in more grains refining of weld metal. Heterogeneous nucleation sites, such as fragmented dendrite tips and partial melted grains remain in the weld pool for more time [5,27]. Owing to increase in cooling rate, the distance among dendrites arm descends from fusion line towards center line of weld and consequently results in more fine grains in weld metal.

All of aforementioned factors cause developing of regions with equiaxed grains from center of weld metal towards the fusion line and decrease in columnar grains (Fig. 3 (a-d)).grains refining and more uniform distribution of precipitates in weld metal were confirmed by SEM images (Fig. 5.) [12,23].

Table 2. Average of length and width of dendrites.

Voltage / The average of	0V	20V	12V	30V
Length of dendrites (µm)	38.86	12.44	22.13	6.05
Width of dendrites(µm)	8.94	3.84	6.55	2.09
Distance between dendrite arms (µm)	12.32	4.92	7.15	3.01
Volume fraction of precipitates (%)	26.02	7.45	16.69	3.06
Size of precipitates (µm)	0.79	0.28	0.49	0.17

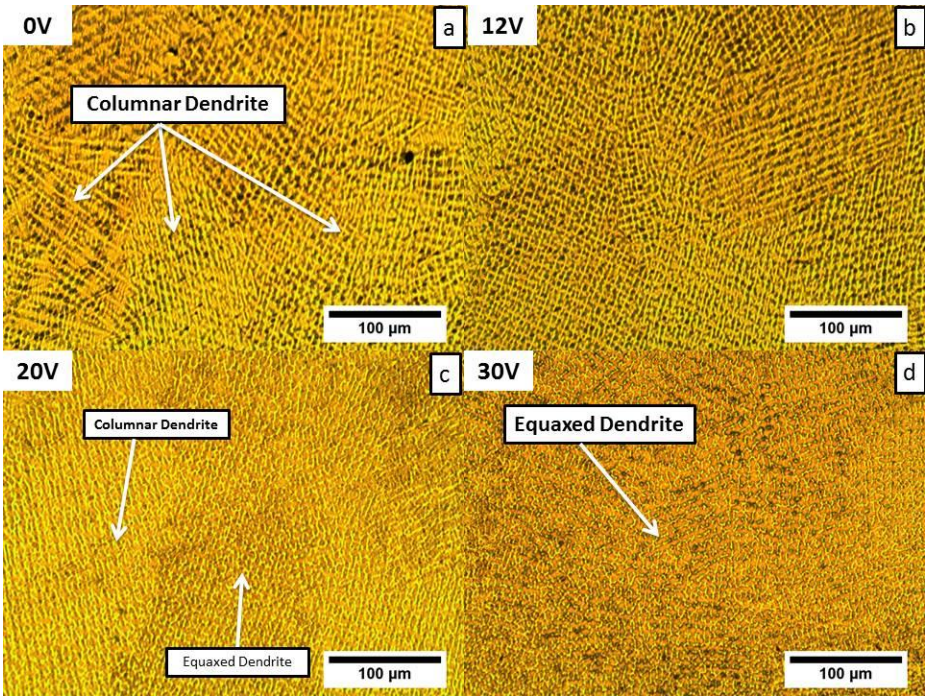

Fig. 3. Images of optical microscope of microstructure of weld metal center a) 0V, b) 12V, c) 20V, d) 30V.

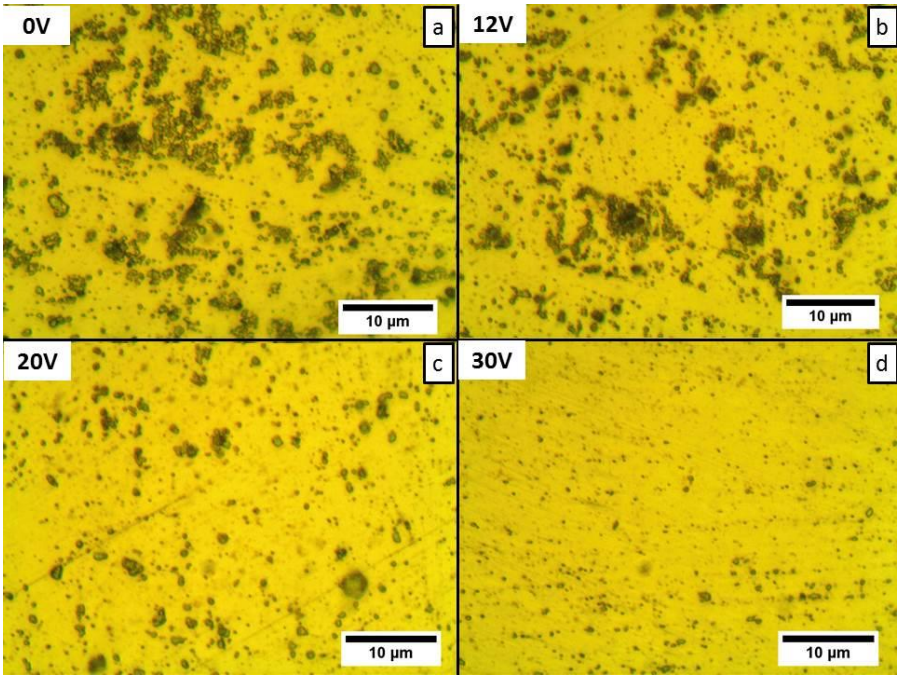

Fig. 4. Images of optical microscope of precipitates distribution a) 0V, b) 12V, c) 20V, d) 30V.

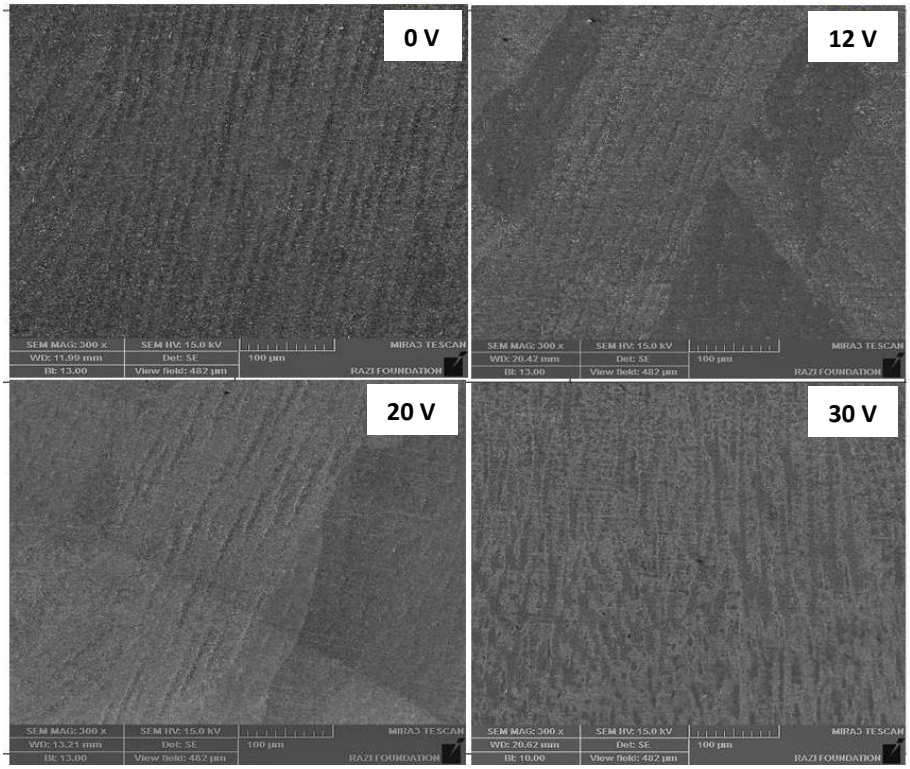

Fig. 5. Images of electron microscope for weld metal microstructure Inconel 82.

3.2. Corrosion

Fig. 6. and Fig. 7. represent the curves of cyclic polarization test on the base and weld metals for different electromagnetic vibrations. The results of these figures are showed in Table 3. For active passive metals, such as stainless steels and superalloys, pitting corrosion is considered as dominant mechanism and evaluation criterion for the present to pitting corrosion these alloys is the E_{pit}-E_{cor} quantity. In this research, the same criterion was used. Fig. 6. shows the polarization test curve for No-vibration weld metal. Analyzing the results in table, reveals that the base metal resistance to pitting corrosion after welding has approximately been remained.

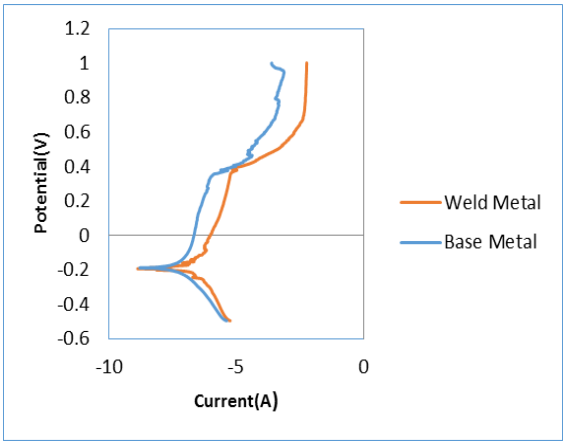

Fig. 6. Polarization test of corrosion base and weld metals.

Vibration causes the grain refinement and more uniform distribution of alloying elements such as Chromium, Nickel and Molybdenum in the structure. Uniform distribution of alloying elements causes the better formation of passive films concurrent with pits formation as a result it prevents formed pit from growing. Presence of inclusions below the passive film causes weakened film and crack growth. For example, existence of the produced inclusions by Titanium, are responsible for pits nucleation [13]. In other words, increasing voltage to 20 V and then 30 V, due to uniform distribution of precipitates and alloying elements, the proper sites for pitting corrosion are decreased and potential drastically increases.

On the other hand, vibration causes the decreasing the grain size and the increasing of grain boundaries density. A result of grain refinement is a drastic increase in the grain boundaries and triple junctions. Grain boundaries have higher energies than the bulk and as such are more chemically active. Increased reactivity coupled with more sites for nucleation of an oxide film on the surface of grain-refined materials is posited to result in a more rapid formation of a protective film [28].

Therefore, it can be caused more cohesion of oxide films (Passive films) to the metal surface and decreases corrosion intensity [29-31]. Refining of structure and uniformity of alloying elements (Fig. 4 (a-d)) prevent from the formation of the unfavorable inclusions and compound on the surface and causes the better cohesion of passive film on the metal surface. Since corrosion in intersection between inclusions and pits is extremely high, therefore vibration, decreases corrosion due to the refining grains and eliminates inclusions and pits [13].

Comparing graphs in Fig. 7. shows that as electromagnetic vibration increases, the graphs tend to arise and it means that corrosion dwindles in a corrosive environment. The graphs of 20 V and 30 V depict the most arise and these mean that the corrosion noticeably decreases. E_{pit} parameter (Table 3.), is pitting potential and augmentation of this parameter represents the improvement of resistance to pitting corrosion [32]. Comparing E_{pit} of samples under vibration with different voltages from 0 V to 30 V reveals that the most magnitude of potential relates to the sample which is vibrated with 30 V (850mV) and the second most one relates to the sample which is vibrated with 20 V (750mV) and these samples are high resistance to pitting. Parameters of the E_{pit}-$E_{cor}$is considered as amount of sensitivity to the pitting corrosion and increase of this expression leads to increase in resistance to pitting corrosion of weld metal from 555.04 (0 V) to 1025.91 (30 V). As it is expected, comparing the results in Table 3. reveals that the more increase in electromagnetic vibration, the more augmentation in (E_{pit}-E_{cor}), which means improvement of resistance to pitting corrosion in samples with voltages 20 V and 30 V [32].

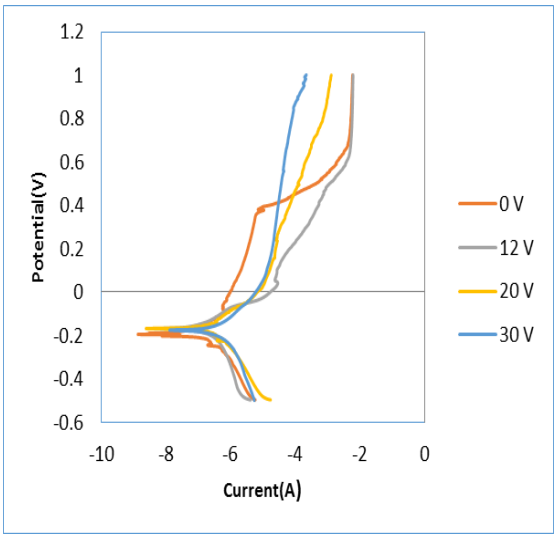

Fig. 7. The graph of polarization test of weld metals.

Table 3. The results of cyclic polarization test for weld metal considering electromagnetic vibration.

Voltages	0 V	12 V	20 V	30 V	Incoloy 825	Inconel 82
E_{Cor} (mV)	-195.04	-168.73	-171.32	-175.91	-185.88	-195.04
E_{Pit} (mV)	360	505	750	850	358	360
$E_{Cor} - E_{Pit}$ (mV)	555.04	673.73	886.32	1025.91	543.88	555.04

4. Conclusions

Based on the results some important results could be concluded as follow:

1. Microstructure of Incoloy 825 superalloy has fully austenitic equiaxed matrix, containing two types of TiC precipitates. First is the TiN with cubical morphology, second is the TiC with spherical morphology inside grains and on the grain boundaries.
2. Applying electromagnetic vibration causes more turbulence of molten and dendrite tips fragmentation and diffusion of them in the molten pool and increasing the heterogeneous nucleation sites. These new sites cause more nucleation of grains and consequently forming finer grains in weld metal.
3. Higher electromagnetic vibration causes the refining grains and increasing the fine equiaxed dendrites. Maximum and minimum of the dendrites average size were 38.86 and 6.05 that revealed to the vibrations, 0 V and 30 V, respectively.
4. Electromagnetic vibration causes the more increasing of grain boundaries in weld metal.. This phenomenon leads to the increasing the connection points of passive films and more cohesion between these films to the metal surface. Therefore, the resistance to pitting corrosion of weld metal is improved.
5. By increasing the vibration intensity, resistance to pitting corrosion of weld metal was increased from 555.04 to 1025.91 mV for vibration of 0 V and 30 V, respectively.
6. Increasing the electromagnetic vibration causes more uniform distribution and finer of precipitates. Maximum and minimum size of precipitates were 0.79 µm (0 V) and 0.17 µm (30 V).

References

[1] E. B. Howard and L. G. Timoty, Desk Edition, Metals Handbook, ASM International, United States of America, (1985).
[2] E.F. Bradly, Superalloys A Technical Guide, 2nd Edition, ASM International, Metalspark, OH44073, (1988).
[3] M.J. Donachie, S.J. Donachie, SuperalloysA Technical Guide, 2nd Edition, ASM International, (2002).
[4] J. R. Davis et al, ASM Specialty Handbook:Nickel, Cobalt, and Their Alloys, Printed in the United States of America, (2000).
[5] R. Dehmolaei, M. Shamanian, A. Kermanpur, Mater.Charact., 59(2008), 1447.
[6] JR. Daris, Metallurgical processing and properties of superalloys. ASM handbooks; 16.18–16-23, (1999).
[7] R. Coppola, S. R. Fiorentin, Nucl. Instrum. Methods. Phys. Res., B22(1987), 564.
[8] Special Metals Corporation, Incoloy Alloy 825, Publication Number SMC-030, (2004).
[9] H. Aytekin, Y. Akcin, Mater. Des., 50(2013),515.
[10] J. C. Lippold, Weld. J., 63(1984), 91.
[11] R. S. Dutta, R. Purandare, A. Lobo and S. K. Kulkarni, Corros. Sci., 46(2004), 2937.
[12] S. Kou: Welding metallurgy, second e.d. , Hoboken, John Wiley & Sons Inc, (2003).
[13] T. Bellezze, G. Roventi andR. Fratesi, Electrochim. Acta, 49(2004), 3005.
[14] P. E. Manning, Corrosion, 36(1980), 468.
[15] F. Cardareli, Materials Handbook.A Concise Desktop Reference, Springer-Verlag London, (2008).
[16] H. Mesmar, E. Gajam, F. E. Zrarrog, Int. J. Adv. Technol. Eng. Res., 5(2015).
[17] K. Balasubramanian, S.Raghavendran and V. Balusamy, Int. J. Eng. Tech. Sci., 2(2011),253.
[18] W.F.Savage, E. F. Nipess andE. S. Szekeres, Weld. J., 55(1976), 260.
[19] R. Dehmolaei, M. Shamanian, Mater.Charact., 60(2009) 246.
[20] M. Sireesha, V. Shankar, SK. Albert and S. Sundaresan, Mater. Sci. Eng. A, 292(2000), 74.
[21] L. Sundar and D. R. G. Achar, Indian Weld. J., 16(1984), 81.
[22] B. Pucko, V.Gliha , Metallurgija, 44(2005), 103.
[23] S. Kou, Y. Le, weld. J., 64(1985), 51.
[24] J.N. DuPont, C.V. Robino and A.R. Marder, Metall. Mater. Trans. A, 29(1998), 2797.
[25] ASTM. A167.99. Standard Specification of Stainless and Heat Resistant Chromium Nickel Steel Plate, Sheet, and Strip.
[26]CH. Vives., JOM, 50(1998).
[27] Y. G. Zhao, Y. H. Liang, Q. D. Qin, W. Zhou and Q. C. Jiang, ISIJ Int., 44(2004), 1167.
[28] K. Ralstone, N. Birbilis, Corrosion, 66(2010), 075005.
[29] E. Sikora, X. J. Wei and B. A. Shaw, Corrosion, 60(2004), 387.
[30] T.C. Tsai, T.H. Chuang, Mater. Sci. Eng. A, 225(1997), 135.
[31] D. Song, A. B. Ma, J. H. Jiang, P. H. Lin and D. H. Yang, T. Nonferr. Metal. Soc., 19(2009), 1065.
[32] M. Amra, K. Ranjbar, and R. Dehmolaei, ASM Int., (2015).